Following the intercalation process of H_2SO_4 into pyrographite by x-ray microscopy

D. Erre,* E. Bourelle, B. Claude-Montigny, A. Métrot, and J. Cazaux
DTI EP120 CNRS, UFR Sciences, Boîte Postale 1039, 51687 Reims Cedex 2, France
(Received 23 December 1996)

A time series of radiographic images with a lateral resolution in the micrometer range has been recorded in order to follow, *in situ*, the intercalation process of H_2SO_4 into pyrographite. The use of x-ray microscopy allows us to visualize and to quantify intercalation fronts inside the specimen giving direct access to intercalation velocities and hence to mobility and diffusion coefficients. The coexistence of various fronts is demonstrated in metastable kinetics situations. [S0163-1829(97)05632-4]

I. INTRODUCTION

More than 70 years after their discovery, a constant interest is taken in intercalation compounds either from the theoretical point of view or for the application purposes. This interest results from the possibility to intercalate a large variety of partly ionized elements or molecules between the layers of lamellar crystals such as graphite, molybdenum, disulphide, etc. Intercalation modifies the properties of the crystal host leading to synthetic materials of adjustable anisotropy. Then, the specific electronic properties of these compounds open fields of applications in catalysis, electrical conduction,[1,2] or more recently, for electrical energy storage, for instance in lithium-ion secondary batteries.[3]

Intercalation compounds are basically characterized by three data, i.e., their chemical composition or stoichiometry, their stage s (number of graphene layers separating two intercalated layers), and the charge of the carbon layers.

This charge is directly deduced from the current integration during electrochemical intercalation while the stage values are determined by *in situ* x-ray diffraction.[4] One problem for such *in situ* characterization is the lack of lateral resolution: x-ray diffractometry provides only global analysis, at best, on areas in the square millimeter range.

Elsewhere the chemical composition is only achieved from *ex situ* sequential microanalyses of samples obtained from quasiequilibrium electrochemical curves. Moreover this procedure may lead to possible intercalant loss during the specimen transfer out of the electrolytic solution. In fact, the most suitable experimental method to follow *in situ* intercalation processes seems presently to be x-ray microscopy if one considers the intrinsic advantages of this technique to observe the bulk of rather thick specimens even set in liquids and its sensitivity for the detection of medium elements embedded in light matrices.[5] This technique has been already used with good results by Anderson Axdal and Chung,[6] and its usefulness has recently been demonstrated by Rondot *et al.* for following the Zn^{2+} ion diffusion in aqueous media.[7] Combined with the speed of the image acquisition brought by a charge-coupled device (CCD) camera used as detector, this technique seems thus particularly convenient to follow the intercalation-deintercalation processes into pyrographite. The corresponding experiments are reported below. The aim of this paper is to show that information can be acquired by x-ray microscopy combined with conventional electrochemical curves.

Electrochemical intercalation of H_2SO_4 into pyrographite has been chosen since it is a well-known process which occurs via stage formation: dense layers of solvated hydrogenosulphate ions successively invade interlamellar spaces of graphite ordered along the c axis [Fig. 1(a)]. The equilibrium potential versus charge curve $E=f(Q=I\tau)$ is characterized by a two-phase plateau alternating with capacitive linear slopes for pure stages.[4] With faster intercalation conditions this curve appears less contrasted suggesting metastable multiphase configurations, as demonstrated using Raman laser spectroscopy for intercalation of Li into TaS_2.[8] Such coexisting intercalation fronts will be investigated here by x-ray microscopy.

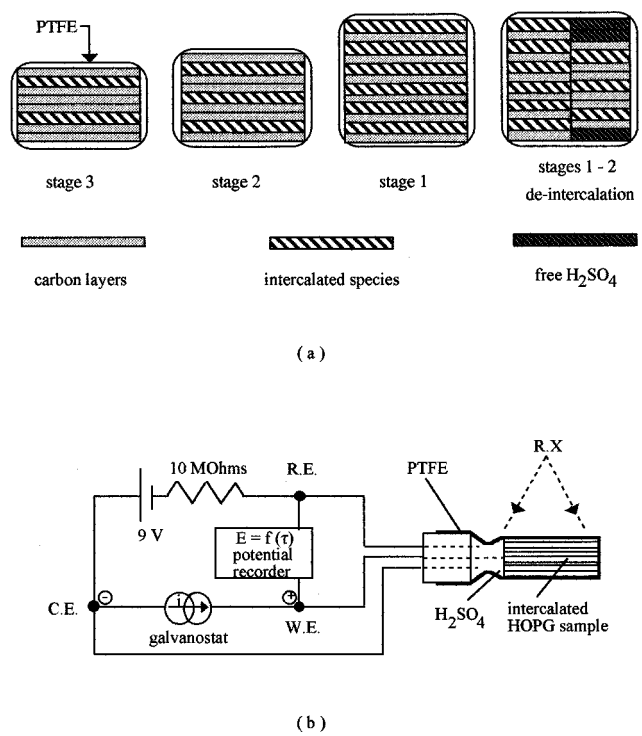

FIG. 1. (a) Cross-section representation of the specimen during the intercalation and deintercalation processes. The stage s corresponds to s layers of HOPG layer for one layer of H_2SO_4. (b) Schematic drawing of the cell: CE, counter electrode; WE, working electrode; RE, reference electrode.

 © 1997 The American Physical Society

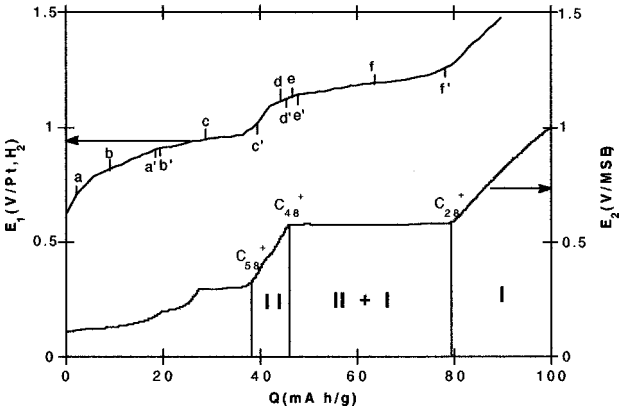

FIG. 2. Experimental $E_1=f(Q)$ curve obtained during the intercalation process of H_2SO_4 into pyrographite. Conventional $E_2=f(Q)$ quasiequilibrium curve (slow operating conditions) is shown as a reference. The intensity was $I=0.5$ mA for a mass of 36.66 mg (fast operating conditions). The various stages are indicated on the $E=f(Q)$ with also the charge values C_{ns}^{+}. The points indicated by a–f on the experimental $E_1=f(Q=I\tau)$ curve correspond to the electrochemical situation for the images of Fig. 3.

II. EXPERIMENTS

In the reported experiment [Fig. 1(b)] the specimen is made of a parallelepipedic highly oriented pyrographite block (HOPG: $5.05\times4.15\times0.80$ mm^3) inserted into a polytetrafluorethylene (PTFE) thermoretractable cell where external walls are 70 μm thick. The cell is filled with 96 % H_2SO_4 (CARLO ERBA, 18 mol l^{-1}) before being hermetically closed (the microscope vacuum is thus protected).

The electrochemical setup includes three classical electrodes [Fig. 1(b)]. A pseudohydrogen reference electrode is realized by negatively polarizing a platinum wire with an electric circuit between this last one and the counter electrode (CE). Two platinum wires crossing the cell wall ensure an electric contact, respectively, with the solution (counter electrode, CE) and the graphite (working electrode, WE). A constant current is applied between WE and CE by means of an external power supply. The curve $E(\text{WE-RE})=f(\tau)$ is continuously plotted during a time series acquisition of x-ray images (Fig. 2, curve 2) (RE is the reference electrode). Due to a limit on beam current (see the next paragraph), to get sufficient signal one must use a large intercalation current (13.6 mA/g) with the consequence of smoothing the experimental $E=f(\tau)$ curve relative to the conventional one (Fig. 2, curve 1). On Fig. 2, curve 2, stage 3 is not clearly distinguishable and equilibrium plateau between stages 3-2 and stages 2-1 are inclined.

The x-ray microscope is of the shadow type. Our original setup is derived from a conventional scanning electron microscope equipped with a cooled CCD camera.[6,7,9] The x-ray beam is generated by the bombardment of a metallic target with a primary electron beam whose energy can vary from 1 to 30 keV. The continuous use of the filament under extreme conditions to have a large beam intensity makes its deterioration very likely and consequently increases the risk of breaking the experiment: it is then necessary to shorten the duration of the experiment as far as possible by increasing the intercalation current. In the vacuum chamber, a target holder permits us to vary the energy of incoming photons by simply using its x movement in order to change the target. A specimen holder allows us to visualize different parts of a sample by moving it in the x-y-z directions.

Depending upon specimen position, the lateral resolution is situated between the x-ray source dimension (around 1 μm) and pixel size (around 25 μm) of each detecting CCD camera element. In the present work, the lateral resolution is around 10 μm. Detection limit of heavy atoms embedded in a weak absorbing medium reaches 10^{-4} atom/atom, and even, 10^{-5} atom/atom in particular cases. The advantage of the experimental arrangement is related to the speed, the good linearity, and the wide dynamic (up to 3×10^4) of the two-dimensional (2D) detector.

Moreover, because these images are acquired and digitally stored, they lead themselves naturally to direct measurement and quantitative analysis of specimen absorptivity at each pixel. Following the well-known Beer law [$I=I_0\exp(-\mu t)$ with μ the linear absorption coefficient and t the specimen thickness] a logarithmic compression of each image permits us to obtain μt maps.[9] Considering that during its intercalation a sample includes along its c axis a constant thickness t_0 of graphene layers and a variable thickness t_i of intercalated species (IS), one can write

$$\mu t=\mu_0 t_0+\mu_i t_i=(\mu t)_0+\Delta\mu t, \tag{1}$$

where μ_0 and μ_i are the linear absorption coefficient of the graphite and of the IS, respectively. The thickness t_i is proportional to the IS quantity so that the composition of the intercalation compound, written as the ratio of the number of intercalated molecules on the number of carbon atoms is

$$c=\frac{\mu_i t_i}{\sigma_i}\frac{\sigma_0}{\mu_0 t_0}=k\Delta\mu t, \tag{2}$$

where σ_0 and σ_i are the cross sections of the graphite and of the IS, respectively, with k a constant if the radiation is considered monochromatic.

Graphite bisulfates are often written as

$$C_{ns}^{+}HSO_4^{-}, \quad xH_2SO_4,$$

where s is the stage number, x and n are factors related to the stoichiometry and to the charge of the compound.

It is noteworthy that intercalated monolayers are quasiliquid with the same density as the free H_2SO_4 (1.83 g/cm^3) and a thickness of 4.65 Å. Comparing these values with the graphite ones (2.2 g/cm^3 and a planar spacing of 3.35 Å) leads to the relation

$$n\approx7(1+x), \tag{3}$$

i.e.,

$$c=\frac{1+x}{ns}\approx\frac{1}{7s}. \tag{4}$$

The μt image acquired at each time of the intercalation process $[(\mu t)_1,(\mu t)_2,\ldots,(\mu t)_n]$ includes the absorption of the wall cell and of the HOPG specimen. But this spurious contribution can be easily removed by subtracting, pixel by pixel, each image $(\mu t)_n$ from the first one $(\mu t)_0$ (acquired at the beginning of the process) in order to obtain [from

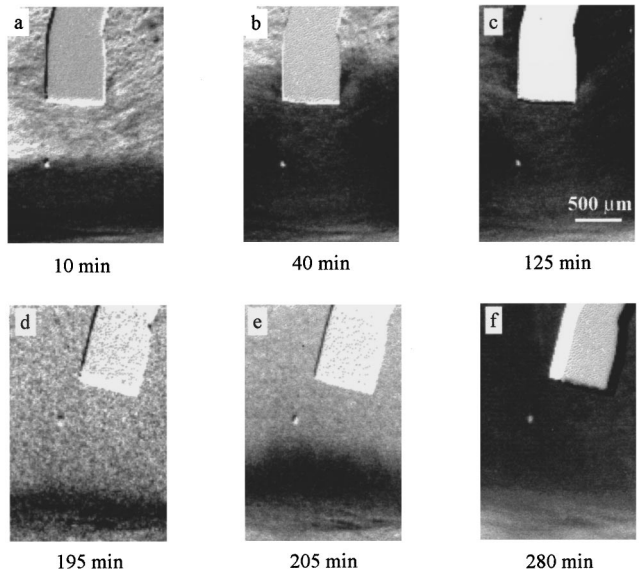

FIG. 3. Examples of images resulting from a logarithmic compression of microradiographies taken at different instants of the intercalation process ($\tau_a=10$ min; $\tau_b=40$ min; $\tau_c=125$ min; $\tau_d=195$ min; $\tau_e=205$ min; $\tau_f=280$ min) and a subtraction, pixel by pixel, from the $\tau=0$ min microradiography for a, b, and c, and from $\tau=185$ min microradiography for d, e, and f, to improve the view of the intercalation front. Here, only the images a, b, and c, correspond to $(\mu t)_n-(\mu t)_0=\Delta\mu t$ and then to the absorption of H_2SO_4; the images d, e, and f, correspond to $(\mu t)_n=(\mu t)_{185}=\Delta\mu t-(\Delta\mu t)_{185}$. The corresponding electrochemical situations a–f, are indicated on Fig. 2. WE is the shadow image of the Pt working electrode having approximately a 650 μm width. We notice that WE moves during the intercalation process as a result of pyrographite swelling.

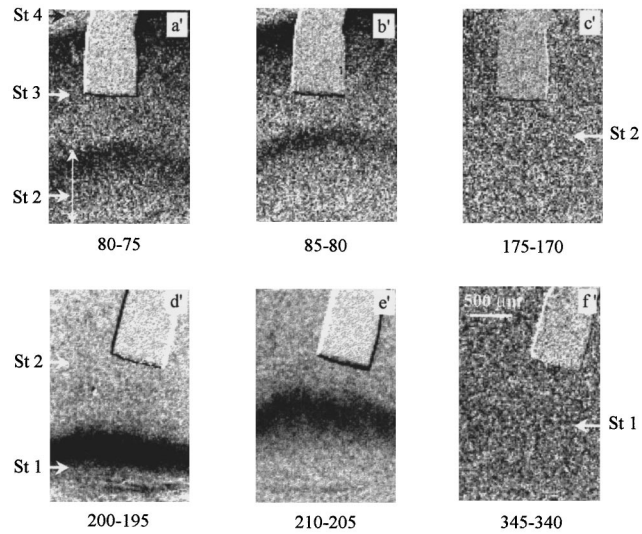

FIG. 4. Difference between two successive μt images $(\mu t)_n-(\mu t)_{n-1}$, in order to outline the progression of the H_2SO_4 fronts (in black). (a′) corresponds to the $\Delta\mu t$ change from $\tau=75$ min to $\tau=80$ min, where three different stages coexist: stages 2, 3, and 4 from bottom to top. The progressions of stages 2 and 3 (in black) are nearly the same. (For their penetration velocity see Fig. 5.) (b′) corresponds to the $\Delta\mu t$ change from $\tau=80$ to 85 min, where the three stages 2, 3, and 4 coexist as in (a). (c′) corresponds to the $\Delta\mu t$ change from $\tau=170$ to 175 min. No significant change is visible: pure stage 2. (d′) corresponds to the $\Delta\mu t$ change from $\tau=195$ to 200 min, where two different stages coexist: stages 1 and 2 from bottom to top. (For the penetration velocity of stage 1 see Fig. 5.) (e′) corresponds to the $\Delta\mu t$ change from $\tau=205$ to 210 min, where stages 1 and 2 (from bottom to top) still coexist. (For the insertion velocity of stage 1 see Fig. 5.) (f′) corresponds to the $\Delta\mu t$ change from $\tau=340$ to 345 min. No significant change is visible: pure stage 1. The corresponding electrochemical situations (a′), (b′), (c′), (d′), (e′), (f′), are indicated on Fig. 2.

$(\mu t)_n-(\mu t)_0]$ the $\Delta\mu t$ value of only the intercalated species according to Eq. (1). Also, the subtraction, pixel by pixel, of two successive images, $(\mu t)_n-(\mu t)_{n-1}$, allows us to visualize the spatial change of the intercalated species between the corresponding acquisition period.

In the present experiment, the total number N of acquired microradiographies was 80; their acquisition time was 1 min and the interval time between two successive images was 5 min. The operating conditions for the x-ray microscope were $I_0=1$ μA; $E_0=30$ keV (primary beam intensity and energy, respectively) and the used radiation was produced with a cobalt target foil, 3 μm thick.

III. RESULTS

Figure 3 presents six images resulting from the difference $(\mu t)_n-(\mu t)_0$ for Figs. 3(a), 3(b), and 3(c) or $(\mu t)_n-(\mu t)_{185}$ for Figs. 3(d), 3(e), and 3(f) (to improve the view of the intercalation front), where $(\mu t)_n$ corresponds to the following acquisition instants (a) $\tau=10$ min, (b) 40 min, (c) 125 min, (d) 195 min, (e) 205 min, and (f) 280. The position of the corresponding electrochemical states a–f are indicated on the experimental potential curve (Fig. 2, curve 2).

Figure 3(a) shows the beginning of the intercalation process with the intercalation of a poor stage (in black) into pristine HOPG (in gray). From the $E=f(\tau)$ curve (Fig. 2, curve 2) the poor stages cannot be analyzed. However, this can be done by x-ray microscopy using Fig. 4(c′) as reference in which there is only the pure stage 2. Indeed, the measured value on the corresponding areas of image 3(c) for the stage 2, is $(\Delta\mu t)_2=1.6$. This experimental value is associated with the theoretical concentration $c_2=7.14\times10^{-2}$ S/C as deduced from Eq. (3).

Then, $(\Delta\mu t)_x=0.35$ for the initial stage x on Fig. 3(a) (in black) corresponds to $c_x=1.56\times10^{-2}$ S/C, i.e., $s\approx9.1$, near stage 9. The deviation between $9(\Delta\mu t)_9$ and $2(\Delta\mu t)_2$ may result from the statistical fluctuations of the counting and from the drift of the incident-beam intensity, in addition to the beam hardening effects associated with the use of the nonmonochromatic beam.

The subtraction $(\mu t)_n-(\mu t)_{n-1}$ is illustrated in Fig. 4. In the usual electrochemical conditions of Figs. 4(a′) and 4 (b′), a mixture of stages 3 and 4 was expected. In actual fact, x-ray microscopy demonstrates that three distinct phases coexist with stage 2, 3, and 4 (from bottom to top). Furthermore, the progression of stage 2 into 3 is similar to that of stage 3 into 4, giving then additional experimental information for this process. The absence of a front on Fig. 4(c′) is consistent with the $E=f(\tau)$ curve where only a pure stage 2 is expected. In fact, during pure stage charging, the acid concentration remains constant, only the ionicity changes

(together with its hydrogen content). In the same way, Figs. 4(d′) and 4(e′) show that stages 2 and 1 coexist and also Fig. 4(f′) proves that stage 1 is a pure stage for $\tau \geqslant 340$ min. The direct view of the process also permits us to observe a front bending that is probably due to the fact that the HOPG sample was more compressed at its borders than at its central part because of the thermoretractable cell, thus preventing the acid access.

IV. DISCUSSION

For each stage, the intercalation velocity can be easily estimated from the measured values of the penetration length d_s (of stage s), at fixed time intervals. From $(\mu t)_n - (\mu t)_{n-1}$ images, d_s experimental values have been plotted as a function of time (open symbols on Fig. 5).

From Fig. 5(a), the penetration velocity of stage 3 into poorer stages p is $v_{3\to p} = (d(d_3)/d\tau = 120/\sqrt{\tau_3}\ \mu\text{m min}^{-1}$ resulting from $d_3 = 240\sqrt{\tau_3}$: the process appears consequently as quasidiffusional. In opposition to this behavior, the progression of stage 1 into stage 2 follows a linear process (Faraday's law) which regression gives $d_1 = 30\tau$ and $v_{1\to 2} = 30\ \mu\text{m min}^{-1}$ [Fig. 5(c)]. Between these extreme situations, the penetration of stage 2 into 3 shows a mixture of these two behaviors and two distinct periods: before and after $\tau_2 = 40$ min [Fig. 5(b)]. Indeed, for $\tau_2 < 40$ min, $(d_2)_1 = 175\sqrt{\tau_2}$ consequently, $(v_{2\to 3})_1 = 87.5/\sqrt{\tau_2}\ \mu\text{m min}^{-1}$ and besides, for $\tau_2 \geqslant 40$ min, $(d_2)_2 = 30\tau_2$ therefore, $(v_{2\to 3})_2 = 30\ \mu\text{m min}^{-1}$. In that case the process is firstly, quasidiffusional and secondly, linear (Faraday's law).

In the same way, apparent diffusion coefficients D of HSO_4^- have also been calculated for quasidiffusional processes considering $v = \sqrt{D/\tau}$. We find for the front advancing of stage 3 into poorer stages $D_3 = 2.4\times 10^{-6}\ \text{cm}^2\,\text{s}^{-1}$, and for that of stage 2 into stage 3, $D_2 = 1.1\times 10^{-6}\ \text{cm}^2\text{s}^{-1}$. Those values are in relative agreement with Fujii's ones deduced from pure electrochemical measurements.[10]

Considering some analogy with Stefan's law for the propagation of fusion-solidification fronts (they progress as the square root of both the time and the temperature deviation), and in the case of a potentiostatic control[11] (which appears here in fast operating conditions with the emergence of a strong overpotential), we have proposed the following law for the penetration speed:

$$v = \sqrt{\nu \Delta E/\tau} \tag{5}$$

where ν is an electrical mobility and ΔE the overpotential. It appears here that $D = \nu\Delta E$ depends of the experimental conditions through ΔE.

Finally, the same procedure was applied during the deintercalation process. X-ray microradiographic images first show a delay of around 25 min between the polarity reversal (of the electrodes) and the beginning of the opposite process. Also, these images (not shown) present a uniform absorption suggesting very curiously that HSO_4^- ions are evacuated continuously from the graphite layer without migration fronts. This phenomenon may be explained considering that the thermoretractable PTFE embedding the sample is suitable to intercalation but not to deintercalation. Indeed, this PTFE irreversibly expanded during intercalation leaves room for the deintercalated acid around HOPG sample (Fig. 1, deintercalation) and this leads to a constant x-ray absorption. But this phenomenon needs further studies to be verified.

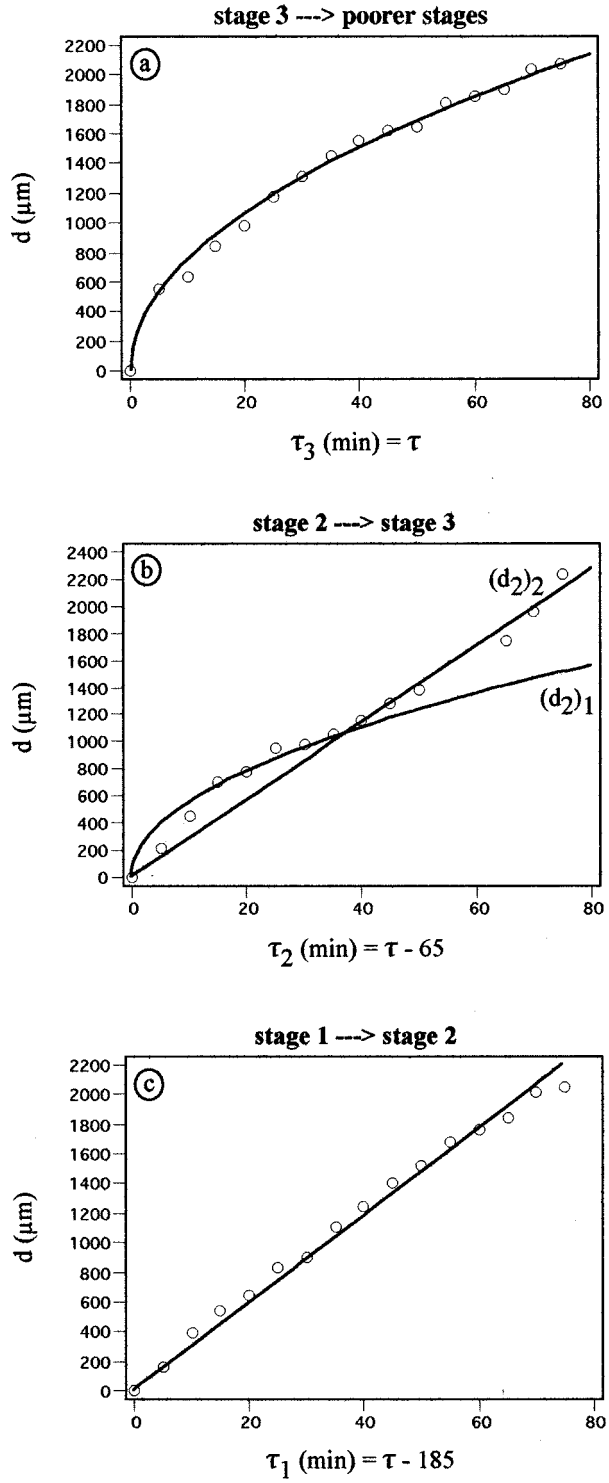

FIG. 5. Penetration length d_s (versus time $\tau_s = \tau - \tau_i$ with τ_i start of stage s): (a) for stage 3 into poorer stages; (b) for stage 2 into stage 3; (c) for stage 1 into stage 2. (Open circles, experimental results; full lines, best fit using root square and linear laws.)

V. CONCLUSION

X-ray microscopy has been used to investigate the *in situ* intercalation process of H_2SO_4 into pyrographite. The coex-

istence of various fronts has been established in metastable kinetic situations; the intercalation velocity of stage s into stage $s+1$ has been measured. Two different regimes for the penetration speed of stage 2 into stage 3 are then suggested and the corresponding diffusion coefficients evaluated.

In the near future, we plan to observe bi-intercalation processes in the presence of two different intercalated species. This seems to be a reasonable aim because of the ability of our technique to map the different components of a given specimen (by using various characteristic radiations).[5,7,9,12] Another possible experiment is to perform x-ray microtomography (i.e., the 3D reconstruction of HOPG block) during the intercalation process in order to visualize in three dimensions the migration front of intercalated species. This last experiment is feasible but it requires the building of a rotating cell.

These examples show that x-ray microscopy as performed with our instrument may open additional fields of investigation in electrochemistry and chemistry in condensed media, where the lack of techniques for microinvestigation is obvious. Its application to electrointercalation may be useful for a better understanding of kinetics mechanisms.

*Electronic address: damien.erre@univ-reims.fr

[1] J. E. Fischer and T. E. Thompson, Phys. Today **36**, 201 (1978).
[2] J. O. Besenhard, H. Möhwald, and J. J. Nickl, Synth. Met. **3**, 187 (1981).
[3] M. Endo, Y. Nishimura, T. Takahashi, K. Takeuchi, and M. S. Dresselhaus, J. Phys. Chem. Solids **57**, 725 (1996).
[4] A. Metrot and J. E. Fisher, Synth. Met. **3**, 201 (1981).
[5] J. Cazaux, H. El Hila, D. Erre, D. Mouze, J. M. Patat, S. Rondot, P. Trebbia, and A. Zolfaghari, in *Electron Microscopy and Analysis 1995*, IOP Conf. Proc. No. 147 (Institute of Physics, London, 1995), Sec. 2, p. 25.
[6] S. H. Anderson Axdal and D. D. L. Chung, Carbon **3**, 377 (1987).
[7] S. Rondot, J. Cazaux, O. Aaboubi, J. P. Chopart, and A. Olivier, Science **263**, 1739 (1994).
[8] T. Butz, A. Lerf, and J. O. Besenhard, Rev. Chem. Min. **21**, 556 (1984).
[9] D. Erre, D. Mouze, X. Thomas, and J. Cazaux, in *X-Ray Optics and Microanalysis 1992*, IOP Conf. Proc. No. 130 (Institute of Physics, London, 1993), p. 567.
[10] R. Fujii, Osaka Kogyo Gijutsu Shikensho Hokoku **353**, 1 (1978).
[11] A. Métrot and M. Tihli, Synth. Met. **23**, 19 (1988).
[12] J. Cazaux, Microsc. Microanal. Microstruct. **4**, 513 (1993).